Spectrochimica Acta Part A: Molecular and Biomolecular Spectroscopy 286 (2023) 122006

Contents lists available at ScienceDirect

Spectrochimica Acta Part A: Molecular and Biomolecular Spectroscopy

journal homepage: www.journals.elsevier.com/spectrochimica-acta-part-a-molecular-and-biomolecular-spectroscopy

A series of phenanthroline-imine compounds: Computational, OLED properties and fluorimetric sensing of nitroaromatic compounds

Ayşegül Kose [a,*], Sultan Erkan [b], Mehmet Tümer [c]

[a] Department of Property Protection and Safety, Elbistan Vocational School, Istiklal University, Kahramanmaras, Turkey
[b] Chemistry Department, Cumhuriyet University, Sivas 58140, Turkey
[c] Chemistry Department, Kahramanmaras Sutcu Imam University, Kahramanmaras, Turkey

HIGHLIGHTS

- Schiff base compounds derived from 5-amino-1,10-phenanthroline were synthesized.
- Crystal structure of compound 1 was determined by single crystal XRD study.
- The sensor properties against nitro-aromatic compounds were investigated.
- Compound **3** showed selective sensing properties for 1,3,5-trinitrophenol.
- Contour diagrams of HOMO/LUMO, non-linear optical (NLO) and OLED properties were investigated by computational studies.

GRAPHICAL ABSTRACT

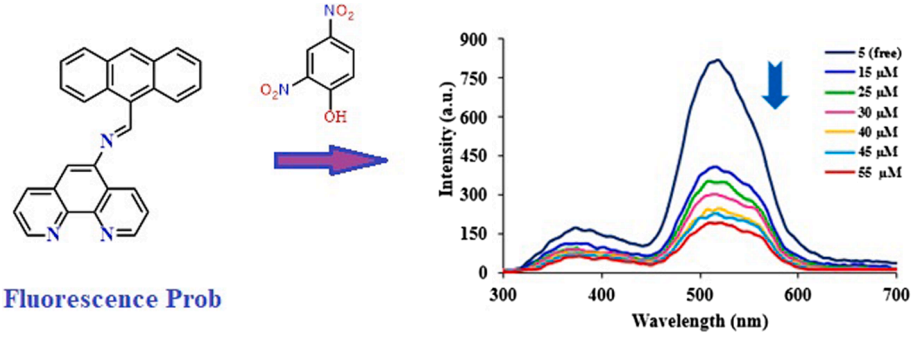

ARTICLE INFO

Keywords:
Schiff base
5-Amino-1,10-phenanthroline
Fluorimetric sensing
Nitroaromatic compounds
DFT
Molecular docking

ABSTRACT

In this study, Schiff base compounds (**1**–**5**) were synthesized by the reaction of 5-amino-1,10-phenanthroline with various aldehydes. The molecular structures of the synthesized compounds were characterized by FT-IR, $^{1}H/^{13}C$ NMR and mass spectroscopic methods. Single crystals of **1** were obtained and their molecular structures in crystalline form were determined by single crystal X-ray diffraction study. The sensor properties of the synthesized compounds against nitroaromatic compounds [nitrobenzene (NB), 4-nitrophenol (NP), 2,4-dintrophenol (DNP) and 1,3,5-trinitrophenol (TNP)] were investigated by fluorescence spectroscopy. Compound **3** have highest sensitivity for the sensing of 1,3,5-trinitrophenol (TNP) (*Ksv*: 4.63×10^4 M^{-1}) with LOD of 4.01 μM while compound **5** showed the highest sensitivity for 2,4-dinitrophenol (DNP) (*Ksv*: 5.71×10^4 M^{-1}) with LOD of 4.75 μM. In addition, the structural parameters (bond angles/lengths), contour diagrams of HOMO/LUMO molecular orbitals, molecular electrostatic potential (MEP) maps, non-linear optical (NLO) and OLED properties were investigated by computational studies. According to the HOMO and LUMO energies, the NLO property of the molecule (**5**) is higher than both other molecules and the reference substance urea.

* Corresponding author.
E-mail address: aysegul.kose@istiklal.edu.tr (A. Kose).

https://doi.org/10.1016/j.saa.2022.122006
Received 12 June 2022; Received in revised form 10 October 2022; Accepted 14 October 2022
Available online 19 October 2022

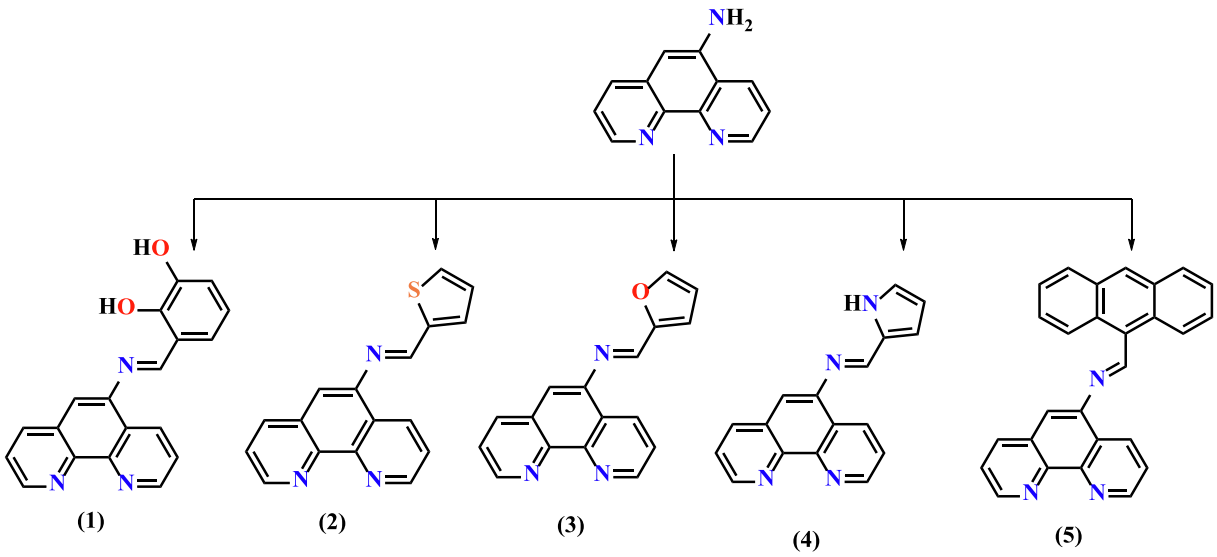

Fig. 1. Phenanthroline based imine compounds **1**–**5**.

1. Introduction

Detection of nitro aromatic compounds (NAC) has been one of the research areas that has attracted attention due to their toxicity and explosive nature [1,2]. The detection of nitroaromatic compounds such as 2,4,6-trinitrotoluene (TNT), 2,4,6-trinitrophenol (TNP) has received special attention due to their explosive nature as well as adverse health problems such as allergies, diarrhoea and neurological disorders [3,4]. In addition, 2,4,6-trinitrophenol (TNP), which has a wide range of applications in the pharmaceutical and paint industries, causes groundwater and soil pollution due to its water solubility due to its acidic character [5,6]. A wide variety of detection methods have been developed to detect nitroaromatic compounds due to both environmental and safety threats [7,8]. Various techniques such as chromatography, membrane electrode technique and spectrophotometric techniques have been investigated for the selective and sensitive detection of nitroaromatic compounds [9]. Methods other than spectrophotometric methods do not have real field applications, are costly and difficult to use [9–11]. In recent years, fluorescence detection, which is a spectrophotometric method, has been applied as an advantageous alternative method in many fields such as biology, pharmacology and environmental sciences [12–15].

Nitroaromatics are considered as nonfluorescent compounds due to the short lifetime of their first singlet excited states [16]. Moreover, fluorescence up-conversion experiments have shown that the rate of fluorescence extinction of nitroaromatic compounds belongs to the femtosecond or picosecond regime [16]. Molecular design is very important in obtaining a selective and sensitive chemosensor [17,18]. Since nitroaromatic compounds contain nitro group, they are electron deficient, and therefore, designing electron-rich molecules facilitates detection of these compounds through better interaction [19,20]. Therefore, polymers with high π-electron conjugation and monomer structures containing polyaromatic groups have been widely used as fluorescence probes in the detection of nitroaromatic compounds [21]. Polyaromatic compounds containing groups such as pyrene, anthracene, naphthalene or phenanthrene in their structures showed significant sensitivity and selectivity in the detection of nitroaromatics [22,23].

In continuance of our interest in fluorescence sensing of nitroaromatic compounds, we prepared five Schiff base compounds (Fig. 1) derived from 5-amino-1,10-phenanthroline and aldehyde derivatives (**1**–**5**). The synthesized compounds were characterized by spectroscopic and analytical methods. Crystal structure of compound (**1**) was determined by single crystal XRD study. Synthesized phenanthroline based compounds were used as fluorescence probes for the sensing of nitroaromatic compounds [Nitrobenzene (NB), 4-nitrophenol (NP), 2,4-dinitrophenol (DNP) and 1,3,5-trinitrophenol (TNP)] were studied in solution.

2. Experimental

All reagents and solvents were of reagent-grade quality and obtained from commercial suppliers (Aldrich or Merck). 5-Nitro-1,10-phenanthroline and 5-amino-1,10-phenanthroline compounds were prepared according to the reported procedures [24].The structural characterization data are provided in the supplementary documents. Elemental analyses (C, H and N) were performed using a LECO CHNS 932. FTIR spectra were obtained using KBr disc (4000–400 cm^{-1}) on a Perkin Elmer Spectrum 400 FT-IR and FTIR spectra of the compounds are provided in the supplementary documents (**Figs. S1-S7**). The electronic spectra in the 200–900 nm range were obtained on a Perkin Elmer Lambda 45 spectrophotometer. ^{1}H and ^{13}C NMR spectra in $CDCl_3$ or DMSO-d_6 were recorded on a Bruker 400 MHz instrument (**Figs. S8-S13**). TMS was used as internal standard. Mass spectra of the ligands were recorded on a LC/MS APCI AGILENT 1100 MSD spectrophotometer (**Figs. S14-S19**).

2.1. Synthesis of phenanthroline-imine compounds (1–5)

Compounds (**1**–**5**) were synthesized according to the reported procedure [25]. 5-Amino-1,10-phenanthroline (0.8 g, 4 mmol) was dissolved in ethanol (10 mL) by heating. The aldehyde compounds (4 mmol) in ethanol (15 mL) were added dropwise to above solution followed by addition of glacial acetic acid (1–2 drops). The solution color changed from yellow to orange-brown with the addition of aldehyde. The resulting solutions were refluxed for 8 h. The progress of the reactions was followed by TLC. After the reactions were complete, the mixtures were cooled to the room temperature. The solvent was removed until the solution volume was 10 mL. The precipitates were filtered and dried in air.

2.2. X-ray crystallography

Single crystals of compound **1** were obtained and single crystal X-ray were collected on Agilent Supernova X-ray single crystal diffractometer. SHELXT 2018/2 and SHELXL-2018/3 programs were used to solve and refine the data[26]. The structure was solved by direct methods and

Table 1
X-ray crystallographic data for compound **1**.

Empirical formula	$C_{20}H_{14}N_3O_2Cl_3$
Formula weight	434.69
Temperature/K	298.0
Crystal system	Monoclinic
Space group	$P2_1/c$
a/Å	8.9509(3)
b/Å	13.2675(4)
c/Å	16.8664(7)
α/°	90
β/°	92.847(4)
γ/°	90
Volume/Å^3	2000.51(12)
Z	4
Crystal size/mm^3	0.18 × 0.12 × 0.08
Radiation	MoKα (λ = 0.71073)
Reflections collected	9560
Independent reflections	4559 [R_{int} = 0.0232, R_{sigma} = 0.0419]
Final R indexes [I>=2σ (I)]	R_1 = 0.0917, wR_2 = 0.2831
Final R indexes [all data]	R_1 = 0.1365, wR_2 = 0.3308
CCDC	2176855

refined on F^2 using all reflections [9]. All non-hydrogen atoms were refined with anisotropic atomic displacement parameters. Hydrogen atoms bonded to carbon and oxygen atoms are placed in the calculated positions. The X-ray crystallographic data are given in Table 1.

2.3. Chemosensing studies against nitro-aromatic compounds

The chemosensory properties of the synthesized compounds against nitroaromatic compounds were investigated by fluorescence spectroscopy. For this purpose, DMSO solutions of nitroaromatic compounds were gradually added to the DMSO solution of the synthesized compounds (by keeping the concentration constant). The emission spectra of the mixtures obtained were taken at the excitation wavelength of the relevant compound and fluorimetric titration was performed. Nitrobenzene (NB), 4-nitrophenol (NP), 2,4-dinitrophenol (DNP) and 1,3,5-trinitrophenol (TNP) were chosen as nitroaromatic compounds. In order to determine the fluorimetric chemosensory activity of the synthesized compounds, the fluorescence quenching constants were obtained using the Stern-Volmer equation [27] given below.

$$I_0/\mathrm{I} = 1 + K_{\mathrm{SV}}[\mathrm{A}]$$

Here; I_0 is the fluorescence intensity of the free compound, I is the fluorescence intensity obtained by adding nitroaromatic, the concentration of [A] nitroaromatic compound and K_{sv} is the quenching constant. The quenching constant K_{sv} is obtained from the slope of the line obtained from the counterplot [A] of I_0/I. The resulting damping constant is a measure of sensitivity. Limit of detection (LOD) for sensing of nitroaromatics were determined by the following equation.

$$\mathrm{LOD} = 3\sigma/\mathrm{k}\,(\sigma: \text{ standard, } \mathrm{k}: \text{ slope}).$$

2.4. Computational procedures

The 3D structures of compounds **1**–**5** were drawn with the program GaussView 6.0.0 [19]. All calculations in the manuscript have been optimized in the gas phase with the Gaussian 09: AS64L-G09RevD.0 program [28] and B3LYP/6-31G(d) level was used for the respective calculations. The energy of the frontier molecular orbitals Equations (1)-(3) are used [29].

$$I = -E_{HOMO} \tag{1}$$

$$A = -E_{LUMO} \tag{2}$$

$$\Delta E = E_{LUMO} - E_{HOMO} \tag{3}$$

To predict the NLO properties, the total static dipole moment (μ), average polarizability (α), polarizability anisotropy (Δα) and total static first hyperpolarizability (β) of compounds **1**–**5** are equations (4)-(7) is calculated from [30].

$$\mu = \left(\mu_x^2 + \mu_y^2 + \mu_z^2\right)^{1/2} \tag{4}$$

$$a = \frac{1}{3}\left(a_{xx} + a_{yy} + a_{zz}\right) \tag{5}$$

$$\Delta a = \frac{1}{\sqrt{2}}\left[\left(a_{xx} - a_{yy}\right)^2 + \left(a_{yy} - a_{zz}\right)^2 + \left(a_{zz} - a_{xx}\right)^2 + 6a_{xz}^2 + 6a_{xy}^2 + 6a_{yz}^2\right]^{1/2} \tag{6}$$

$$\beta = \left[\left(\beta_{xxx} + \beta_{xyy} + \beta_{xzz}\right)^2 + \left(\beta_{yyy} + \beta_{yzz} + \beta_{yxx}\right)^2 + \left(\beta_{zzz} + \beta_{zxx} + \beta_{zyy}\right)^2\right]^{1/2} \tag{7}$$

OLED properties are determined using the Marcus theory. The electron (λe) and hole (λh) reorganization energies of chemical species are determined by Marcus theory. The relation given by Equations (8)-(9) is found from the neutral, cationic and anionic single point energy of the compounds. In addition to this, a series of single point energies are calculated. [31,32].

$$\lambda_e = \left(E_0^- - E_-^-\right) + \left(E_-^0 - E_0^0\right) \tag{8}$$

$$\lambda_h = \left(E_0^+ - E_+^+\right) + \left(E_+^0 - E_0^0\right) \tag{9}$$

Where E_0^+ and E_0^- are the energies of the cation and anion of neutral molecule. E_+^+ and E_-^- are the energies of the cation and anion obtained from cation and anion. E_+^0 and E_-^0 are the energy of the neutral molecule calculated at the cationic and anionic state. E_0^0 is the energy of the neutral molecule at the ground state.

Another parameter are adiabatic/vertical ionization potentials (IPa/IPv) and adiabatic/vertical electron affinities (EAa/EAv) [33]. These parameters are obtained from Equation (11)-(14).

$$IPa = E_+^+ - E_0^0 \tag{10}$$

$$IPv = E_0^+ - E_0^0 \tag{11}$$

$$EAa = E_0^0 - E_-^- \tag{12}$$

$$EAv = E_0^0 - E_0^- \tag{13}$$

Here E_0^- and E_0^+ are the energy of the re-optimized anion (cation). E_-^- (E_+^+) is the energy of the anion (cation) calculated with the optimized anion (cation) structure, E_-^0 (E_+^0) is the energy of the neutral molecule calculated at the anionic (cationic) state. In addition, E_0^0 is defined as the energy of the neutral molecule at the ground state [34].

3. Results and discussion

In this work, five Schiff base compounds **1**–**5** derived from 5-amino-1,10-phenanthroline and aldehyde compounds were prepared by condensation reactions. The structure of the compounds was characterized by FT-IR, ^{1}H/^{13}C NMR, mass spectroscopies and elemental analysis. The compounds were obtained in high yield and purity. All compounds are soluble in common organic solvents such as methanol, ethanol, chloroform, DMF and DMSO and not soluble in water. The elemental analysis data of the compounds are in good agreement with the proposed structure of the compounds.

FTIR spectra of the compounds were taken and the characteristic stretching peaks were investigated. In the spectrum of starting 5-amino-1,10-phenanthroline, the peaks observed in the spectrum of the compound at 1633, 1610, 1595 cm^{-1} were attributed to the ν(N-H), ν(C=$N_{phenanthroline}$) and ν(C=C) bond stretching's, respectively. When

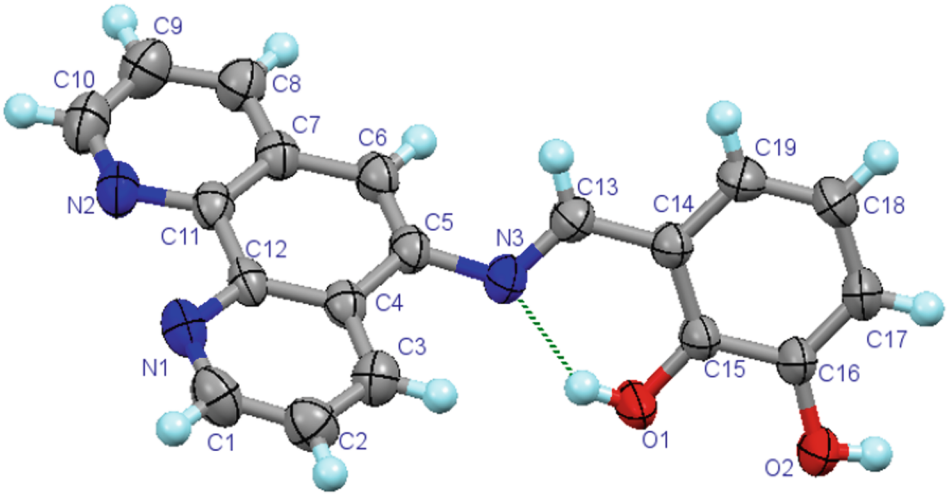

Fig. 2. Molecular structure of compound **1** (thermal ellipsoid with 50% probability).

the FTIR spectra of Schiff base compounds (**1**–**5**) were examined, it was observed that the peak originating from the free amino group $\nu(NH_2)$ in the starting material disappeared. Instead, a new sharp peak in the range of 1599–1633 cm^{-1} are due to the imine bond stretching's $\nu(C{=}N_{imine})$ confirming the formation of Schiff base compounds. The broad bands observed in the spectrum of compound (**1**) in the range of 3300–3500 cm^{-1} are due to the phenolic groups ν(O-H). The $\nu(C{=}N_{phenanthroline}$ stretching peak in the spectra of the compounds were observed in the range of 1563–1595 cm^{-1}. The FTIR spectra of the compounds are provided in the supplementary documents.

The ESI-Q-TOF mass spectra of the compounds were taken in methanol. The mass spectral data for the compounds are given in the supplementary documents. When the mass spectra of the Schiff base compounds were examined, molecular ion peaks $[M+H]^+$ or $[M+Na]^+$ were observed with high the relative abundance values. The ESI-Q-TOF mass spectra of the compounds are provided in the supplementary documents.

3.1. NMR spectra

The $^1H/^{13}C$ NMR spectra of the starting 5-Amino-1,10-phenanthroline and its Schiff base derivatives **1**–**5** were taken in $CDCl_3$ or DMSO-d_6 in order to make structural characterizations of the synthesized compounds and to detect the absence of organic impurities in the structures. $^1H/^{13}C$ NMR data of the compounds are given in the supplementary document. NMR spectra of the compounds are provided in the supplementary documents. In the ^1H NMR spectrum of 5-amino-1,10-phenanthroline, doublet signals due to the aromatic protons were observed at 9.21, 8.96, 8.29 and 8.00 ppm. In the spectrum of the compound, a triplet signal at 7.52 a singlet signal at 6.94 ppm was also observed. The ^1H NMR spectral data of 5-amino-1,10-phenanthroline is in good agreement with reported values. A broad peak observed at 4.29 in the spectrum of the compound is assigned to the free -NH_2 group protons. When the ^1H NMR spectra of Schiff base compounds **1**–**5** were examined, the proton (CH=N) of the imine bond was observed as singlet signal in the range of 9.15–9.35 ppm. The phenolic group protons of

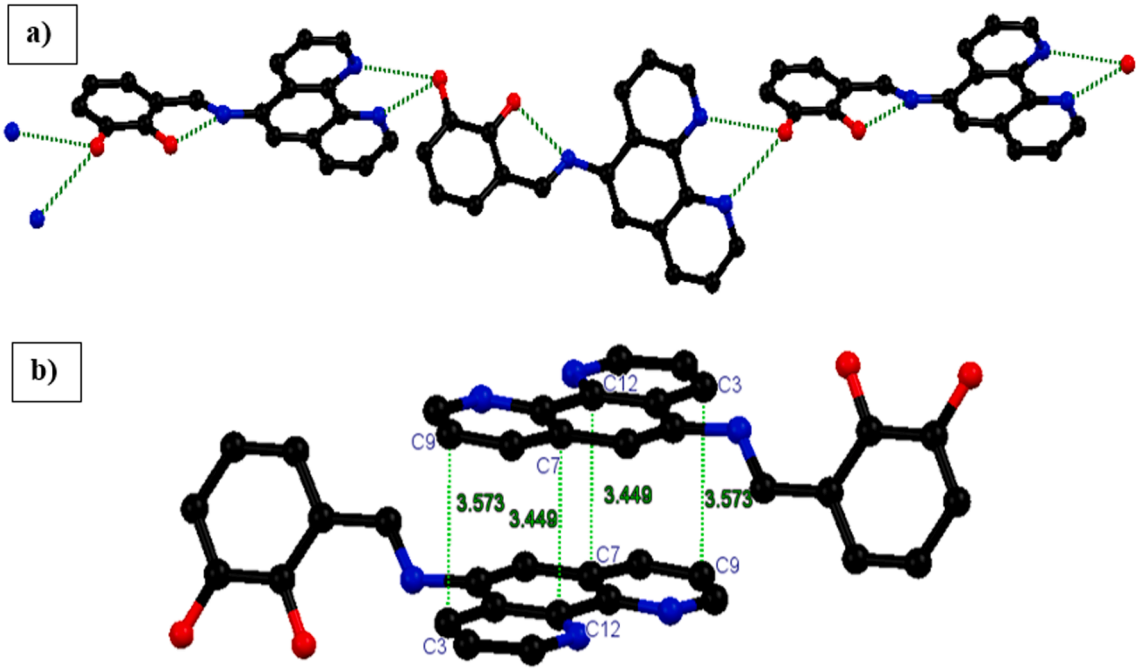

Fig. 3. a) Hydrogen bond chain in structure of **1**. **b**) π-π stacking interactions in **1**.

compound **1** were observed as broad bands at 12.36 and 10.27 ppm. A broad signal observed at 12.06 ppm in compound **4** was due to the -NH- proton in the pyrrole ring. In the spectra of compounds **1**–**4**, aromatic proton signals in the phenanthroline, thiophene, pyrrole and furan rings were observed as multiple peaks in the range of 9.05–6.30 ppm. In the ^{1}H NMR spectrum of compound **5**, the aromatic proton signals in the anthracene and phenanthroline rings in the structure were mostly observed as overlapped multiplets. A singlet signal at 9.37 ppm was assigned to the proton of anthracene group in the para-position with respect to the imine bond. The singlet peak observed at 9.35 ppm in the spectrum of the compound originated from the imine bond (CH=N) proton. The number of proton atoms in the structure of all synthesized compounds is compatible with the integration values of the signals observed and no significant organic impurities was observed in the compounds.

In the ^{13}C NMR spectra of the 5-amino-1,10-phenanthroline, twelve aromatic carbon atom signals were observed in the range of 150.07–105.51 ppm and ^{13}C signals of the compound are compatible with its structure. In the spectra of the Schiff base compounds **1**–**5**, a carbon atom signal due to the imine bond (C=N) carbon atom was observed in the range of 165–155 ppm. Aromatic carbon atoms in the Schiff base compounds were observed in the range of 150.79–102.02 ppm. The number of carbon atom signals observed in the spectra of all Schiff base compounds are consistent with their proposed structures.

3.2. Molecular structure of compound *1*

Single crystals of Schiff base compound **1** were obtained by slow evaporation in chloroform solution. Single crystal X-ray diffraction data of the compound were collected and the molecular structure in solid form was solved. The molecular structure of the compound is given in Fig. 2. According to X-ray data, there is one chloroform solvent molecule per Schiff base molecule in the crystal lattice of the compound and thus the asymmetric unit contains a Schiff base compound **1** and a chloroform solvent. The crystal structure of the compound is solved in the monoclinic unit cell and the P21/c space group. In the compound, the 1–10-phenanthroline and dihydroxybenzene units are linked by imine bond. The length of the imine bond (N3-C13) is 1.277(5) Å and has the character of a C=N double bond. In addition, the C-O bond length for the hydroxyl (-O1H) group, which is in the ortho position with respect to the azomethine bond in the benzene ring, is 1.352(4)Å and has the characteristic C-O single bond distance. According to the data obtained from X-ray diffraction study, it was determined that the compound crystallized in phenol-imine tautomeric form.

A bending angle of 60.68° was observed between the approximately planar phenanthroline and phenol units in the compound. As expected, the compound has a phenol-imine (O1-H····· N3) intramolecular hydrogen bond. The second phenolic group (-O2H) in the molecule involves in a bifurcated intermolecular hydrogen bond with the phenanthroline nitrogen atoms of a neighbouring molecule (Fig. 3**a**). These intermolecular hydrogen bonds have formed a one-dimensional hydrogen bond chain. In addition, the planar phenanthroline ring in the compound entered into head–tail type π-π interaction with the same group in the neighbouring molecule (Fig. 3**b**). The observed intermolecular hydrogen bonds and π-π interactions formed a two-dimensional supramolecular structure. Solvent molecules are located in the lattice spaces formed in this supramolecular structure (**Fig. S20**). In addition, the hydrogen atom of each chloroform solvent molecule placed in the lattice spaces entered into C-H·····π interaction with the centre of the phenolic group in the compound. The interaction distance of the hydrogen atom of the solvent molecule interacting with the centre of the benzene ring is 2.563 Å.

3.3. UV–Vis absorption and emission properties

UV–Vis absorption and photoluminescence properties of the compounds in solution (DMSO, 10^{-5} M) were investigated and spectral data are presented in Table 2. The absorption and photoluminescence spectra of the compounds are given in Fig. 4. In the absorption spectrum of 5-amino-1,10-phenanthroline, an absorption band observed at λ_{max}: 257 nm can be assigned to the π-π* electronic transitions of the π-electrons in the structure. Moreover, there are two not well separated weaker bands observed at λ_{max}: 286 and 307 nm and these bands are due to the π-π* and n-π* electronic transitions, respectively. When the absorption spectra of Schiff base compounds **1**–**5** were examined, the shifts were observed in both absorption values and wavelengths, these reflects the presence different groups attached to the phenanthroline. The absorption bands of all Schiff base compounds showed hyperchromic shifts with respect to the 5-amino-1,10-phenanthroline. In the spectrum of compound **1** and **3**, two absorption bands observed at 245–410 nm were observed and these bands are assigned to the π-π* and n-π* electronic transitions, respectively. In the spectra of compounds **2** and **4**, the absorption band of π-π* transitions at 245–320 nm range are accompanied by a shoulder band at λ_{max}: 281 nm. In the spectrum of **4**, n-π* transitions were not observed. In the spectrum of compound **5**, in addition to the strong absorption band at 245–310 nm range due to the π-π* transitions, two weaker bands were observed at 350–450 nm range (λ_{max}: 365 and 415 nm). These two absorption bands are characteristic electronic transitions of anthracene group [9].

Table 2
UV–Vis absorption and photoluminescence data of the compounds.

Compound	UV–Vis. (λ_{max}, nm)	Exc. (λ_{max}, nm)	Em. (λ_{max}, nm)
5-Amino-1,10-phenanthroline	257, 286, 307	257	430
1	268, 337	266	305, 365
2	260, 281, 341	258	305, 366
3	278, 356	278	311, 369
4	257, 281	256	312, 367
5	260, 369, 415	262	323, 356

The photoluminescence properties of the 5-amino-1,10-phenanthroline and its Schiff base derivatives **1**–**5** were also investigated in DMSO (10^{-5} M) (Fig. 4). All compounds are emissive when excited at their corresponding maximum absorption values of π-π* transitions. Upon excitation at 257 nm, 5-amino-1,10-phenanthroline showed a broad emission band in the range of 370–500 nm (λ_{max}: 430 nm). Although the Schiff base compounds **1**–**5** are excited at similar wavelengths to that of 5-amino-1,10-phenanthroline, they showed significantly different emission properties. In the spectra of the compounds **1**–**5**, the emission band in the range of 370–500 nm due to the starting 5-amino-1,10-phenanthroline showed red-shift with significant quenching's. Instead, the Schiff compounds emits light in the range of 260–420 nm upon irradiated at 258–278 nm range. The emission spectra of compounds **2** and **4** are similar and showed strong emission band at 275–350 nm range accompanied by a shoulder band. The emission spectra of the compounds **1** and **3** are similar to those of **2** and **4**, yet emission intensities are significantly lower. Compound **5** exhibits two almost separated emission maximums in the range of 275–410 nm. The emission spectra of the compound **5** is similar to those compounds containing the anthracene moiety [9].

3.4. Optimized structures and structural parameters

The optimized structures of **1**–**5** compounds were obtained in gas phase at the level of B3LYP/6-31G(d) and are given in Fig. 5 and some molecular structure parameters of the investigated compounds are presented in Table 3.

When structural parameters of compounds **1**–**5** given in Table 3 are examined, it is remarkable that the molecular structures basically do not change in the same bound group phenanthroline part. For each molecule, the C1-N1 bond length is approximately 1.2 Å and the C2-N2 bond

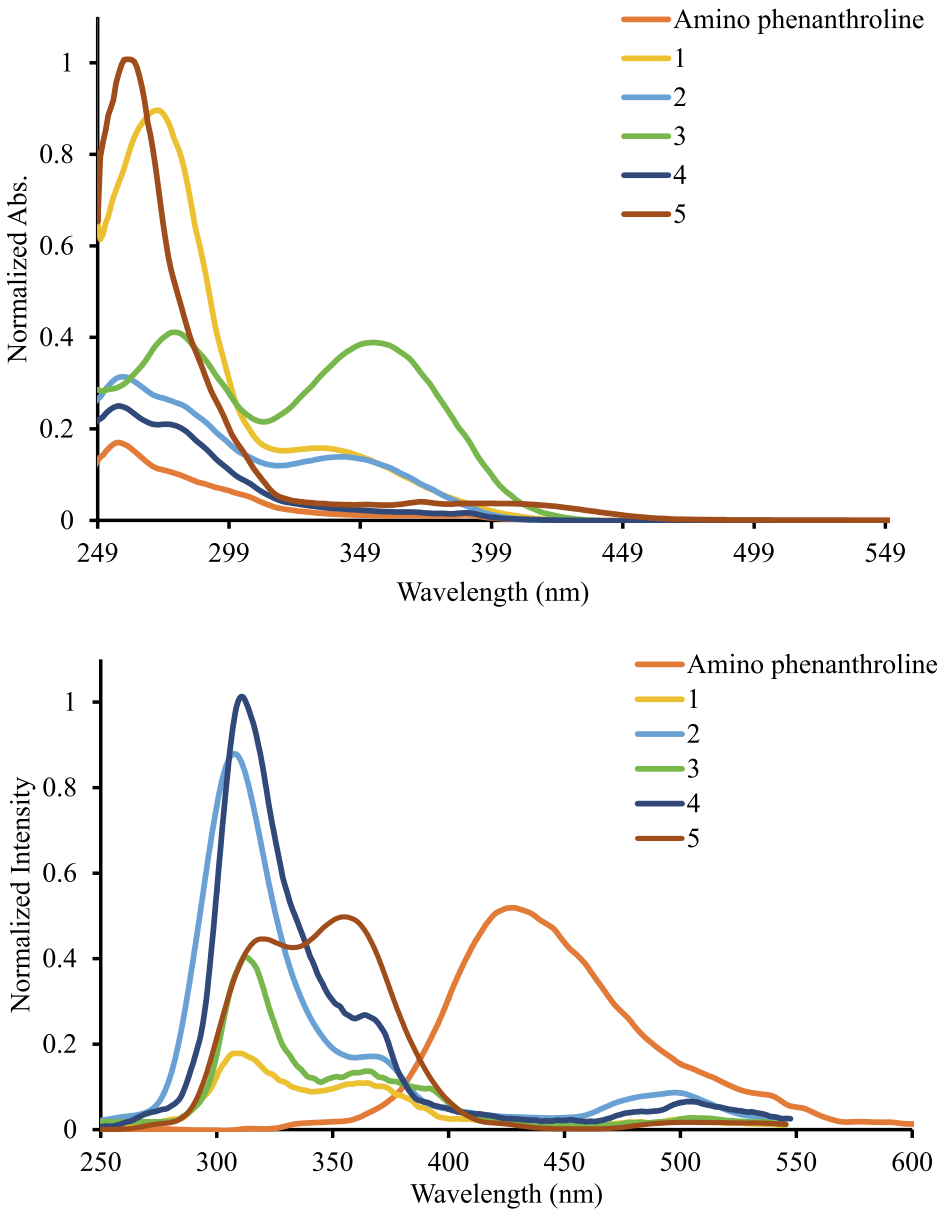

Fig. 4. Normalized absorption (up) and emission spectra of the synthesized compounds in DMSO (10^{-5} M).

length is 1.4 Å. This situation is compatible with the double bond and single bond structure formed by the nitrogen donor atoms with the carbon atom. In addition, the C1-N1-C2 bond length was calculated to be approximately 120° and it shows that the steric and inductive effects of the groups attached to the nitrogen atom attached to the phenanthroline moiety do not have an important role in the molecular structure.

3.5. Frontier molecular orbitals

According to Molecular Orbital Theory, the highest occupied molecular orbital (HOMO) and lowest energy unoccupied molecular orbital (LUMO) energies can be used to characterize the electron donating and electron accepting capacity of the chemical species. High values of a molecule's HOMO energy indicate that it has a good electron donating potential and a low LUMO orbital energy indicates that the molecule has a good electron accepting potential. Frontier molecular orbital images and energy gaps of the studied molecules are given in Fig. 6.

According to the contour diagrams of the HOMO and LUMO orbitals given in Fig. 6, it shows that the HOMO and LUMO orbitals are localized in the π-bonds of the molecules. The HOMO molecular orbital refers to the electron donating sites in the molecule. Electron donor atoms in molecules appear on the phenanthrene moiety and electron acceptor atoms are on alternating ligands in molecules.

3.6. NLO properties

Molecules with nonlinear optical (NLO) properties can change the propagation properties of incoming light (phase, frequency, amplitude, polarization, etc.). Therefore, molecules with NLO properties attract attention. Computational chemistry techniques can correlate NLO properties of molecules with numerical data. Especially organic molecules have attracted much attention due to their various strategies such as conjugated system and planarity.

Quantum chemical parameters and polarizability parameters (total static dipole moment (μ), mean linear polarizability (α), anisotropy of polarizability (Δα), and first hyperpolarizability (β)) are used to estimate NLO properties [30]. The total static dipole moment (μ), mean linear polarizability (α), anisotropy of polarizability (Δα) and first

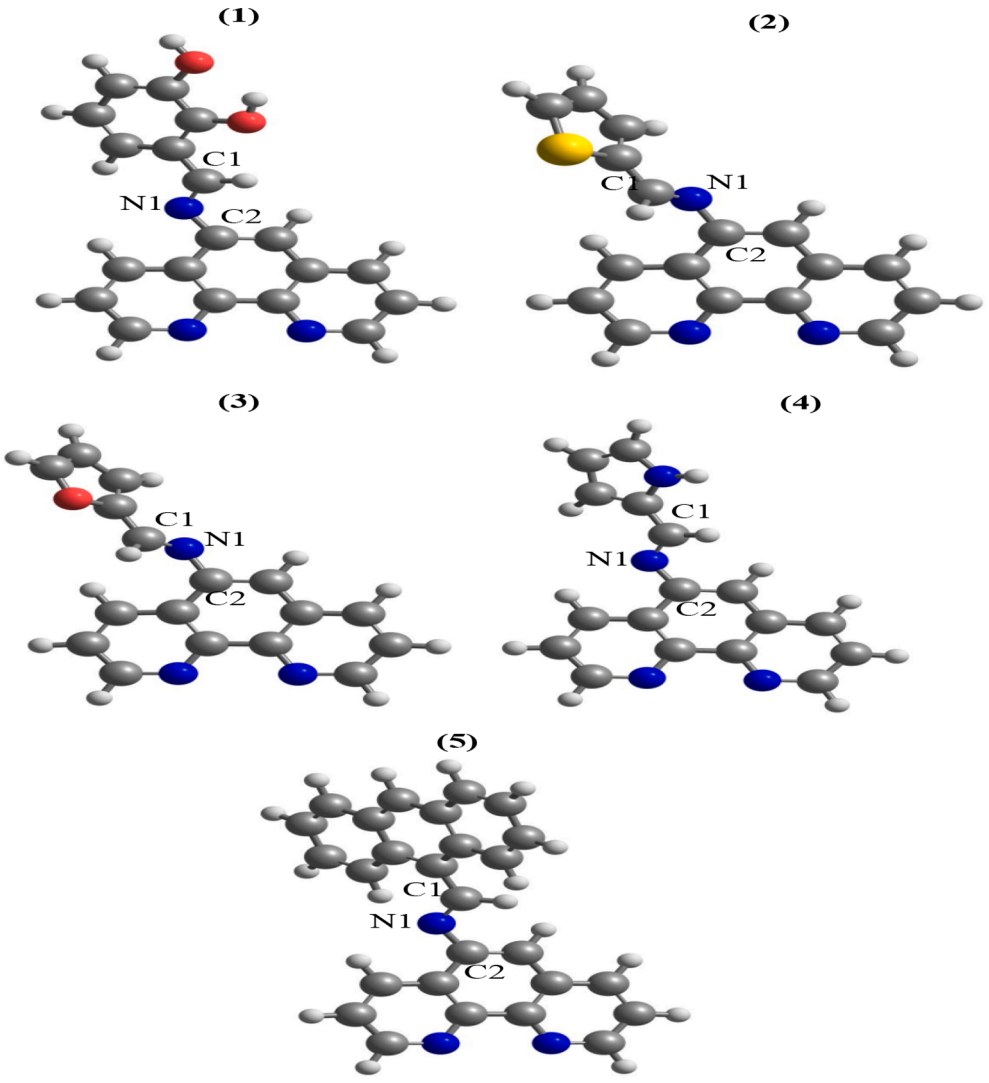

Fig. 5. Optimized structures of investigated compounds.

Table 3
Some calculated structural parameters for compounds **1**–**5.**

Compounds	Bond Length (Å)		Angle Degree (°)
	C1-N1	C2-N2	C1-N1-C2
1	1.284	1.401	119.7
2	1.282	1.406	120.4
3	1.283	1.406	120.4
4	1.286	1.397	119.7
5	1.287	1.400	119.4

hyperpolarizability (β) values for molecules **1**–**5** are calculated at the B3LYP/6-31G(d) level. NLO properties can be associated with the parameters given in **Table S1**. If the HOMO energy is high, the electron transfer tendency may increase. A lower ELUMO value indicates higher electron accepting ability of the molecule. The NLO properties of the studied molecules become advantageous with increasing HOMO and decreasing LUMO energy values. Moreover, if the energy difference between LUMO and HOMO decreases, the NLO properties of the molecules increase [35]. According to the HOMO and LUMO energies, the NLO property of the molecule **5** is higher than both other molecules and the reference substance urea, and this may indicate that the compound **5** has more NLO properties.

Total static dipole moment(μ), mean linear polarizability (α), polarizability anisotropy (Δα) and first hyperpolarizability (β) values given in **Table S1** are the basic parameters in predicting NLO properties. The NLO properties of the investigated compounds are compared with the urea reference material. Increasing values of these parameters provide superiority in terms of NLO materiality. According to the results listed in **Table S1**, the NLO parameters of compound **5**, whose π delocalization is evident, are quite high, and the NLO order of the investigated compounds is **5** > **1** > **4** > **3** > **2**.

3.7. Light emitting properties

We can get information about OLED material properties of chemical species with computational chemistry methods. OLED material properties can be evaluated in many ways. An OLED device has layers with different properties. The suitability of the OLED material for any of these layers can be predicted by some parameters. These layers consist of an electron transport layer (ETL), an emission layer (EL), and a hole transport layer (HTL) between a cathode and an anode. In addition to these layers, there is the electron injection layer (EIL) adjacent to the cathode and the hole injection layer (HIL) adjacent to the anode. The reference material for ETL compounds is tris(8-hydroxyquinoline) aluminum complex (Alq3) [36]. Preparation and characterization of blue-luminescent tris (8-hydroxyquinoline)-aluminum (Alq3). while the reference material for HTL compounds is N,N'-diphenyl-N,N'-. bis(3-

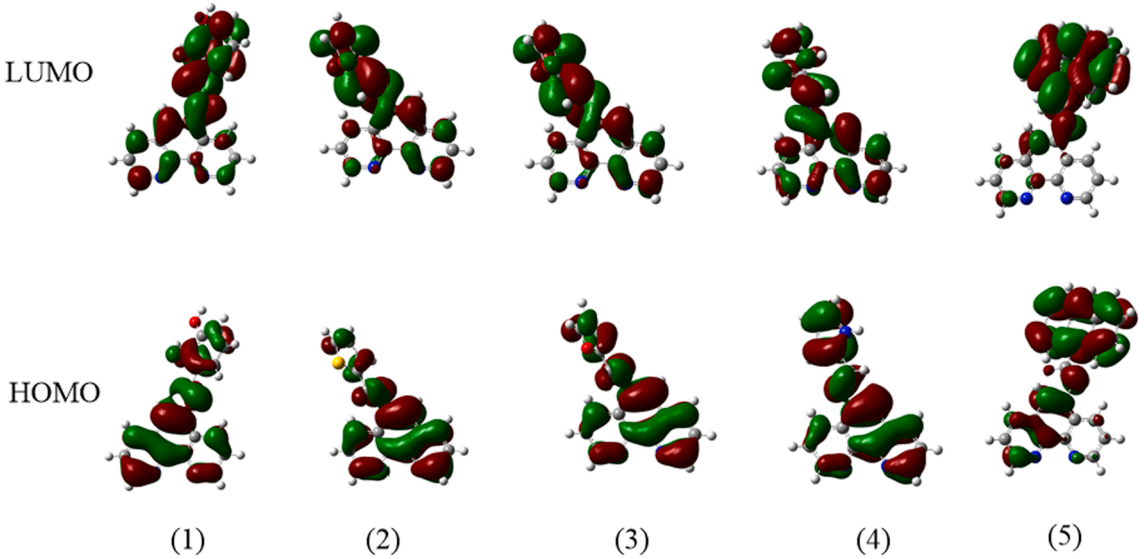

Fig. 6. Frontier molecular orbitals of compounds**1**-**5.**

methylphenyl)-1,1′-diphenyl-4,4′-diamine (TPD) [37]. Photoluminescence and electroluminescence of the exciplex formed between a terbium ternary complex and N, N′-diphenyl-N, N′-bis (3-methylphenyl)-1, 1′-diphenyl-4, 4′-diamine. A good OLED material should have parameters superior to reference materials.

To apply the Marcus equation to molecules, eight energy parameters per molecule given in Equations (9) and (10) were calculated with the level of B3LYP/6-31G(d) (**Table S2**). The parameters obtained and the reorganization energies (λ_e and λ_h) in **Table S2** were obtained from the equations. The suitability of compounds **1**–**5** to the OLED material layers can be judged by comparing them with those of the reference materials. For ETL material, reference Alq3 (λ_e = 0.276 eV) is used, for HTL material reference TPD (λ_h = 0.290 eV) is used. The lower the reorganization energy than the reference materials suggest that it will have a

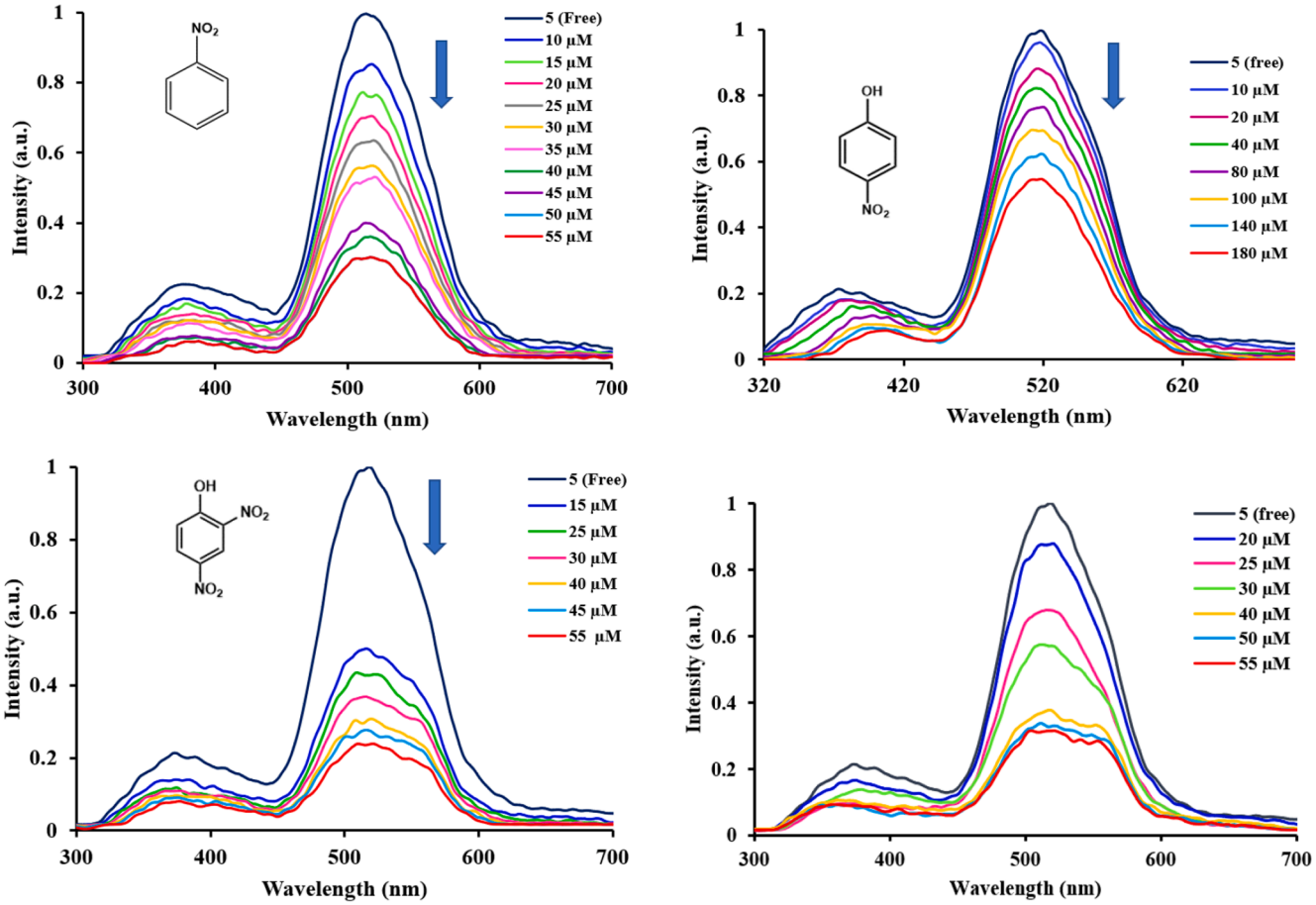

Fig. 7. The normalized emission spectra of compound **5** in DMSO (10^{-5} M) upon addition of different concentrations of nitroaromatic in DMSO (λ_{exc}: 262 nm).

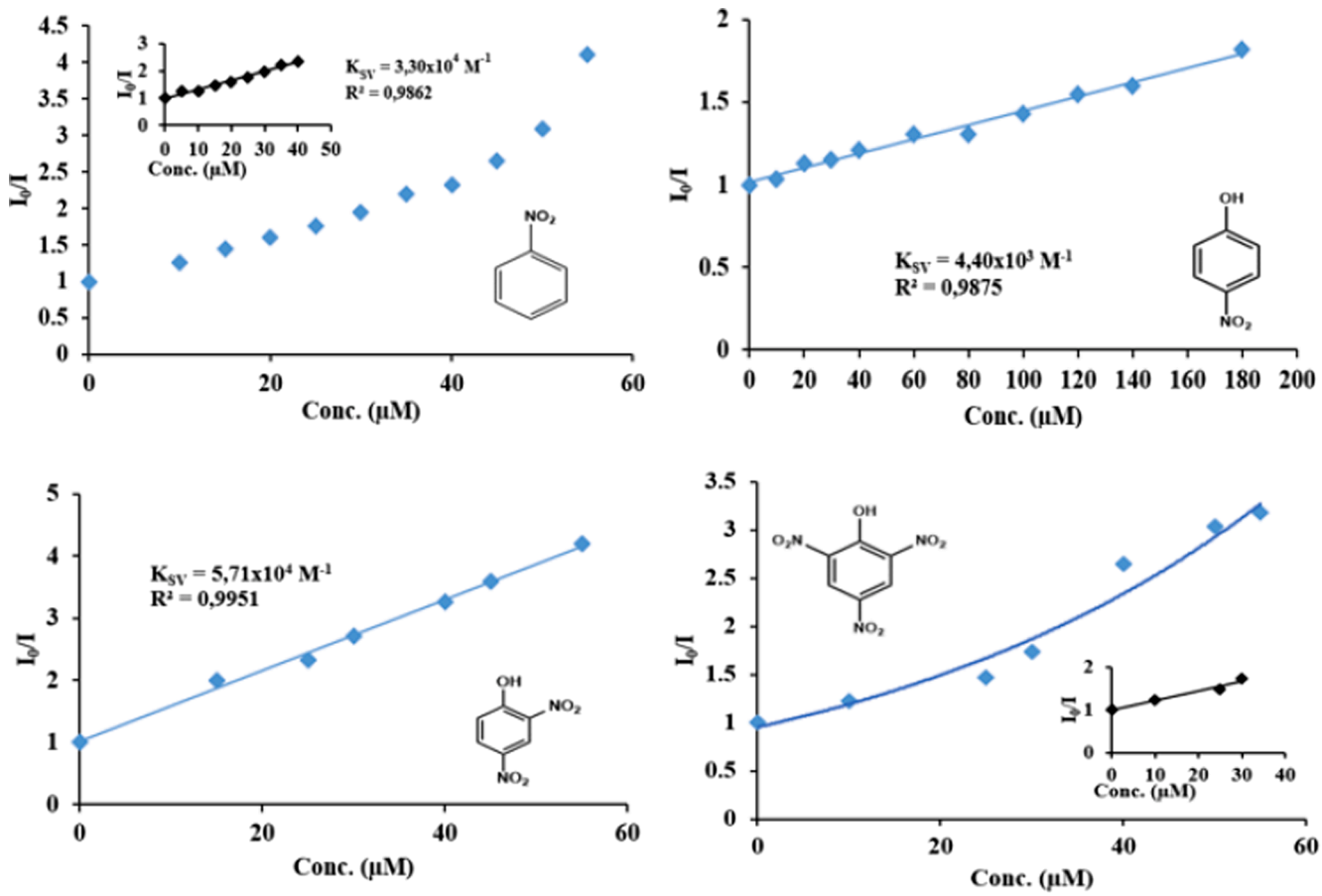

Fig. 8. The Stern-Volmer plots of **5** with NB, NP, DNP and TNP. The solid lines were fitted to the concentration-resolved data using the Stern-Volmer equation. Insets in the graph of NB and TNP are linear part of The Stern-Volmer plots obtained for 0–40 µM concentration range.

higher charge transfer rate. With this approach, its suitability for ETL and HTL material can be suggested. The calculated electron and hole reorganization energies of compound **5** are 0.109 and 0.219 eV, respectively. The calculated electron and hole reorganization energies of compound **1** are 0.152 and 0.265 eV, respectively. The λe of compounds **5** and **1** are lower than the reference Alq3 (λ_e = 0.276 eV) [38]. Efficiency and stability of different tris (8-hydroxyquinoline) aluminium (Alq3) derivatives in OLED applications. Therefore, it can be said that compounds **5** and **1** are more advantageous as ETL materials instead of Alq3. In **Table S2**, only the λ_h values of compounds **5** and **1** for the HTL material are smaller than the λ_h value of TPD (λ_h = 0.290 eV). Only these two molecules are suitable for HTL material. Hole injection capacity can be correlated with IP and EA values. In general, molecules with smaller IP and larger EAs allow easier injection of holes from the hole (electron) transport layer to the emitter layers. In this way, it facilitates hole and electron transfer. **Table S2** shows the adiabatic/vertical ionization potentials (IPa/IPv) and adiabatic/vertical electron affinities (EAa/Eav) values of the molecules. The IPa/v and EAa/v values of **5** are 4.118/4.165 eV and 0.892/0.901 eV, respectively. The IPa/v and EAa/v values of (1) are 4.461/4.299 eV and 0.894/0.885 eV, respectively. When the results are examined, the IP values of **5** are lower than the others. Again, the EA values of **5** are higher than the others. The order of advantage of the investigated compounds as HIL and EIL compounds is almost similar to the order of NLO properties, and the general trend among the compounds is **5** > **1** > **4** > **3** > **2**.

3.8. Fluorimetric sensing properties towards nitroaromatic compounds

Fluorescent quenching-based fluorimetric sensors are one of the selective and sensitive methods that have been frequently studied in recent years for the detection of nitro-aromatic explosives [17]. The quenching effect occurs in the emission band mainly due to the interaction of the fluorescence sensor with the nitroaromatic compound. There are many reported fluorescence quenching-based fluorimetric sensors for the detection of nitroaromatic compounds in the literature. However, reported fluorimetric probes reported have significant disadvantages such as high cost, multi-step synthesis, reusability, lack of selectivity, and low sensitivity. The sensor properties of the synthesized Schiff base compounds (**1**–**5**) were investigated by fluorescence spectroscopy in the detection of nitroaromatic compounds. DMSO solutions of nitroaromatic compounds with varying concentrations (0–100 M) were added to the DMSO solution of the synthesized compounds (keeping probe concentration constant). The emission spectra of each probe in the presence of different nitro-aromatic concentration were measured and changes in the emission spectra were taken into account. Nitrobenzene (NB), 4-nitrophenol (NP), 2,4-dinitrophenol (DNP) and 1,3,5-trinitrophenol (TNP) were used as nitroaromatic compounds. Gradual addition of nitrobenzene (NB), 4-nitrophenol (NP), 2,4-dinitrophenol (DNP) and 1,3,5-trinitrophenol (TNP) generally caused decreases in fluorescence emission intensities (quenching) of all compounds. As representative, the emission spectra of the compound **5** in the presence of various nitroaromatics are shown in Fig. 7. However, it has been found that each fluorescent compound has different sensitivity quenching constants to different nitroaromatics and thus sensory properties.

Based on the emission quenching of the compounds in the presence of different nitroaromatic compounds, the quenching constants (*Ksv*) were calculated from the slope obtained from the Stern-Volmer equation (I_0/I versus nitroaromatic concentration [A]). The linearity of the Stern-Volmer plots suggest the static quenching mechanism by a ground state charge transfer between the nitroaromatics and probes. As

Table 4
Ksv and LOD values for the detection of nitroaromatic compounds.

K_{sv} M^{-1} (R^2) Compounds	NB	NP	DNP	TNP
1	2.67 × 10^4(0.9884)	1.02 × 10^4(0.9948)	2.80 × 10^4(0.9974)	1.97 × 10^4(0.9900)
2	3.25 × 10^4(0.9872)	3.80 × 10^3(0.9929)	2.29 × 10^4(0.9728)	4.13 × 10^4(0.9826)
3	9.80 × 10^3(0.9922)	6.00 × 10^3(0.9749)	5.26 × 10^4(0.9996)	4.63 × 10^4(0.9975)
4	2.60 × 10^4(0.9898)	2.90 × 10^3(0.9826)	1.14 × 10^4(0.9933)	1.63 × 10^4(0.9982)
5	3.30 × 10^4(0.9862)	4.40 × 10^3(0.9875)	5.71 × 10^4 (0.9951)	2.26 × 10^4(0.9604)
Limit of detections (LOD, μM)				
	NB	**NP**	**DNP**	**TNP**
1	36.30	26.20	11.76	36.85
2	5.48	21.45	26.66	6.13
3	22.45	9.50	2.00	4.01
4	2.64	13.27	6.41	9.54
5	6.47	13.00	4.75	7.43

representative, I_0/I versus nitroaromatic concentration [A] graphs for compound **5** are shown in Fig. 8. The quenching constants (*K*sv) are given in Table 4. The magnitude of the *K*sv values is indicative of their sensitivity to the studied nitroaromatics. As the magnitude of the damping constant increases, the sensitivity increases. As can been seen from Table 4, all compounds showed quenching based sensor properties toward studied nitroaromatics and their sensitivities (*K*sv) are 2.90 × 10^3-5.71 × 10^4 M^{-1} range. The relatively *K*sv values of the compounds **1**–**5** compared to the literature suggest the poor binding interactions between the fluorophore and analyte [39,40]. When *K*sv values are taken into account, all compounds showed higher sensitivity to 2,4-dinitrophenol (DNP) and 1,3,5-trinitrophenol (TNP) than the other nitroaromatics. For the sensing of 2,4-dinitrophenol (DNP) the best sensitivity was obtained for compound **5** with *K*sv value of 5.71 × 10^4 M^{-1}. For compound **5**, the order of sensitivity for the sensing of nitroaromatics is DNP > NB > TNP > NP. The higher sensitivity of compound **5** towards DNP may be due to the better energy transfer in the excited between the DNP and probe **5**.

Compound **3** have highest sensitivity for the sensing 1,3,5-trinitrophenol (TNP) (*K*sv: 4.63 × 10^4 M^{-1}). Relatively higher sensing abilities of the synthesized compounds towards 2,4-dinitrophenol (DNP) and 1,3,5-trinitrophenol (TNP) are due to the better energy transfer in the excited state from excited molecules to the nitroaromatics. It has been interpreted that the excited state energy level of the synthesized compounds may be close to the lowest energy vacant orbital energy level of electron-poor DNP or TNP, and this allows more efficient energy transfer resulting in higher quenching constants. The similar observations were observed in previous studies [30].

Finally, the limits of detection (LOD) of the synthesized compounds were calculated and given in Table 4. Micro molar level of detection was obtained for our molecules as pertinent with other reported fluorescence probes. For the sensing of 2,4-dinitrophenol (DNP) and 1,3,5-trinitrophenol (TNP), compound **3** showed the lowest LOD values 2.00 and 4.01 μM, respectively. It has been seen that the obtained LOD values are comparable to the values in the literature [9,30,41].

4. Conclusions

A series of 1,10-phenanthroline based Schiff base compounds were prepared and their structures were determined by spectroscopic and analytical methods. The compounds were used as small fluorescence probes for the sensing of nitroaromatic compounds. All compounds showed fluorescence quenching based sensory properties, yet no specific selectivity towards any of nitroaromatics used. Compound **3** exhibited sensitivity for 1,3,5-trinitrophenol (TNP) with *K*sv: 4.63 × 10^4 M^{-1} and compound **5** has the highest sensitivity for 2,4-dinitrophenol (DNP) with *K*sv: 5.71 × 10^4 M^{-1}). Lowest LOD was found for compound **3** for sensing of DNP with LOD of 2.00 μM. Non-linear optical (NLO) and OLED properties of the compounds were investigated by computational studies. According to the HOMO and LUMO energies, compound **5** showed the NLO property than both other molecules and the reference substance urea.

CRediT authorship contribution statement

Ayşegül Kose: Writing – original draft, Conceptualization, Methodology, Data curation, Investigation. **Sultan Erkan:** Writing – original draft, Investigation, Data curation. **Mehmet Tümer:** Supervision, Project administration, Data curation.

Declaration of Competing Interest

The authors declare that they have no known competing financial interests or personal relationships that could have appeared to influence the work reported in this paper.

Data availability

Data will be made available on request.

Acknowledgments

Authors would like to thank to Kahramanmaraş Sütçü İmam University project coordination unit for providing financial support (Project number: 2019/6-16D). Authors also thank to Scientific and Technological Research Council of Turkey (TÜBİTAK 2211A PhD scholarship) and Higher Education Institution (YOK 100/2000 Sensor Technologies) for providing scholarship support to A.K.

Appendix A. Supplementary data

Supplementary data to this article can be found online at https://doi.org/10.1016/j.saa.2022.122006.

References

[1] J.S. Yang, T.M. Swager, Fluorescent porous polymer films as TNT chemosensors: Electronic and structural effects, J. Am. Chem. Soc. 120 (1998) 11864–11873, https://doi.org/10.1021/ja982293q.
[2] V. Bhalla, A. Gupta, M. Kumar, D.S.S. Rao, S.K. Prasad, Self-assembled pentacenequinone derivative for trace detection of picric acid, ACS Appl. Mater. Interfaces. 5 (2013) 672–679, https://doi.org/10.1021/am302132h.
[3] F. Abbasi, A. Akbarinejad, N. Alizadeh, CdS QDs/N-methylpolypyrrole hybrids as fluorescent probe for ultrasensitive and selective detection of picric acid, Spectrochim. Acta - Part A Mol Biomol. Spectrosc. 216 (2019) 230–235, https://doi.org/10.1016/j.saa.2019.03.032.
[4] M. Hussain, A. Nafady, S. Sirajuddin, S.T. Hussain Sherazi, M.R. Shah, A. Alsalme, M.S. Kalhoro, S.A. Mahesar, S. Siddiqui, Cefuroxime derived copper nanoparticles and their application as a colorimetric sensor for trace level detection of picric acid, RSC Adv. 6 (86) (2016) 82882–82889.
[5] W.L. Goodfellow, D.T. Burton, W.C. Graves, L.W. Hall, K.R. Cooper, Acute Toxicity of Picric Acid and Picramic Acid To Rainbow Trout, Salmo Gairdneri, and American Oyster, Crassostrea Virginica, JAWRA J. Am. Water Resour. Assoc. 19 (1983) 641–648, https://doi.org/10.1111/j.1752-1688.1983.tb02782.x.
[6] R. Dheepika, R. Abhijnakrishna, P.M. Imran, S. Nagarajan, High performance p-channel and ambipolar OFETs based on imidazo[4,5-: F] -1,10-phenanthroline-triarylamines, RSC Adv. 10 (2020) 13043–13049, https://doi.org/10.1039/d0ra00210k.
[7] A.C. Schmidt, B. Niehus, F.M. Matysik, W. Engewald, Identification and quantification of polar nitroaromatic compounds in explosive-contaminated waters by means of HPLC-ESI-MS-MS and HPLC-UV, Chromatographia 63 (2006) 1–11, https://doi.org/10.1365/s10337-005-0703-8.
[8] H. Dong, W. Gao, F. Yan, H. Ji, H. Ju, Fluorescence resonance energy transfer between quantum dots and graphene oxide for sensing biomolecules, Anal. Chem. 82 (2010) 5511–5517, https://doi.org/10.1021/ac100852z.
[9] M. Kose, H. Kırpık, A. Kose, Fluorimetric detections of nitroaromatic explosives by polyaromatic imine conjugates, J. Mol. Struct. 1185 (2019) 369–378.
[10] G. He, H. Peng, T. Liu, M. Yang, Y. Zhang, Y. Fang, A novel picric acid film sensor via combination of the surface enrichment effect of chitosan films and the

aggregation-induced emission effect of siloles, J. Mater. Chem. 19 (2009) 7347–7353, https://doi.org/10.1039/b906946a.
[11] T.M. Swager, The Molecular Wire Approach to Sensory Signal Amplification, Acc. Chem. Res. 31 (1998) 201–207, https://doi.org/10.1021/ar9600502.
[12] D. Wu, A.C. Sedgwick, T. Gunnlaugsson, E.U. Akkaya, J. Yoon, T.D. James, Fluorescent chemosensors: The past, present and future, Chem. Soc. Rev. 46 (2017) 7105–7123, https://doi.org/10.1039/c7cs00240h.
[13] P. Devibala, R. Dheepika, P. Vadivelu, S. Nagarajan, Synthesis of Aroylbenzoate-Based Push-Pull Molecules for OFET Applications, ChemistrySelect. 4 (2019) 2339–2346, https://doi.org/10.1002/slct.201803394.
[14] E.V. Verbitskiy, Y.A. Kvashnin, A.A. Baranova, K.O. Khokhlov, R.D. Chuvashov, I. E. Schapov, Y.A. Yakovleva, E.F. Zhilina, A.V. Shchepochkin, N.I. Makarova, E. V. Vetrova, A.V. Metelitsa, G.L. Rusinov, O.N. Chupakhin, V.N. Charushin, Synthesis and characterization of linear 1,4-diazine-triphenylamine–based selective chemosensors for recognition of nitroaromatic compounds and aliphatic amines, Dye. Pigment. 178 (2020) 1–10, https://doi.org/10.1016/j.dyepig.2020.108344.
[15] L.R. Adil, P. Gopikrishna, P. Krishnan Iyer, Receptor-Free Detection of Picric Acid: A New Structural Approach for Designing Aggregation-Induced Emission Probes, ACS Appl. Mater. Interfaces. 10 (2018) 27260–27268, https://doi.org/10.1021/acsami.8b07019.
[16] R. Morales-Cueto, M. Esquivelzeta-Rabell, J. Saucedo-Zugazagoitia, J. Peon, Singlet Excited-State Dynamics of Nitropolycyclic Aromatic Hydrocarbons: Direct Measurements by Femtosecond Fluorescence Up-Conversion, J. Phys. Chem. A 111 (2007) 552–557, https://doi.org/10.1021/jp065364d.
[17] X. Sun, Y. Wang, Y. Lei, Fluorescence based explosive detection: from mechanisms to sensory materials, Chem. Soc. Rev. 44 (2015) 8019–8061, https://doi.org/10.1039/C5CS00496A.
[18] R. Chennoufi, H. Bougherara, N. Gagey-Eilstein, B. Dumat, E. Henry, F. Subra, S. Bury-Moné, F. Mahuteau-Betzer, P. Tauc, M.P. Teulade-Fichou, E. Deprez, Mitochondria-targeted Triphenylamine Derivatives Activatable by Two-Photon Excitation for Triggering and Imaging Cell Apoptosis, Sci. Rep. 6 (2016) 1–12, https://doi.org/10.1038/srep21458.
[19] J.M.M. R.D. Dennington II, T.A. Keith, GaussView 5.0, Wallingford CT. (2009).
[20] R. Dheepika, A. Shaji, P.M. Imran, S. Nagarajan, Improving device performance of p-type organic field-effect transistor using butterfly like triarylamines, Org. Electron. 81 (2020), 105568, https://doi.org/10.1016/j.orgel.2019.105568.
[21] B. Pramanik, N. Singha, D. Das, Sol-, Gel-, and Paper-Based Detection of Picric Acid at Femtogram Level by a Short Peptide Gelator, ACS Appl. Polym. Mater. 1 (2019) 833–843, https://doi.org/10.1021/acsapm.9b00071.
[22] S. Kumar, R. Kishan, P. Kumar, S. Pachisia, R. Gupta, Size-Selective Detection of Picric Acid by Fluorescent Palladium Macrocycles, Inorg. Chem. 57 (2018) 1693–1697, https://doi.org/10.1021/acs.inorgchem.7b02813.
[23] P.P. Kumavat, P.K. Baviskar, B.R. Sankapal, D.S. Dalal, Facile synthesis of D-π-A structured dyes and their applications towards the cost effective fabrication of solar cells as well as sensing of hazardous Hg(ii), RSC Adv. 6 (2016) 106453–106464, https://doi.org/10.1039/c6ra18712a.
[24] K. Binnemans, P. Lenaerts, K. Driesen, C. Görller-Walrand, A luminescent tris(2-thenoyltrifluoroacetonato)europium(<scp>iii</scp>) complex covalently linked to a 1,10-phenanthroline-functionalised sol–gel glass, J. Mater. Chem. 14 (2004) 191–195, https://doi.org/10.1039/B311128H.
[25] W. Chen, N.B. Zuckerman, J.P. Konopelski, S. Chen, Pyrene-functionalized ruthenium nanoparticles as effective chemosensors for nitroaromatic derivatives, Anal. Chem. 82 (2010) 461–465, https://doi.org/10.1021/ac902394s.
[26] I.A.H.A. Sherwani, A. Köse, Ö. Güngör, H. Kırpık, S.A. Güngör, M. Köse, Synthesis, characterization and investigation of photophysical and biological properties of Cu (II) and Zn(II) complexes of benzimidazole ligands, Appl. Organomet. Chem. 36 (4) (2022) e6585, https://doi.org/10.1002/aoc.6585.
[27] K. Campbell, A. Zappas, U. Bunz, Y.S. Thio, D.G. Bucknall, Fluorescence quenching of a poly(para-phenylene ethynylenes) by C 60 fullerenes, J. Photochem. Photobiol. A Chem. 249 (2012) 41–46, https://doi.org/10.1016/j.jphotochem.2012.08.015.
[28] D.J.F. M.J. Frisch, G.W. Trucks, H.B. Schlegel, G.E. Scuseria, M.A. Robb, J.R. Cheeseman, G. Scalmani, V. Barone, B. Mennucci, G.A. Petersson, H. Nakatsuji, M. Caricato, X. Li, H.P. Hratchian, A.F. Izmaylov, J. Bloino, G. Zheng, J.L. Sonnenberg, M. Hada, M. Ehar, Gaussian, Inc., Wallingford CT. (2010).
[29] S. Erkan, Activity of the rocuronium molecule and its derivatives: A theoretical calculation, J. Mol. Struct. 1189 (2019) 257–264, https://doi.org/10.1016/j.molstruc.2019.04.042.
[30] S.A. Gungor, I. Sahin, O. Gungor, S.E. Kariper, F. Tumer, M. Kose, Pamoic acid esters and their xanthene derivatives: Flourimetric detection of nitroaromatic compounds and non-linear optical properties, Sensors Actuators, B Chem. 255 (2018) 3344–3354, https://doi.org/10.1016/j.snb.2017.09.161.
[31] U. Daswani, U. Singh, P. Sharma, A. Kumar, From Molecules to Devices: A DFT/TD-DFT Study of Dipole Moment and Internal Reorganization Energies in Optoelectronically Active Aryl Azo Chromophores, J. Phys. Chem. C 122 (2018) 14390–14401, https://doi.org/10.1021/acs.jpcc.8b04070.
[32] N. Özkan, S. Erkan, K. Sayın, D. Karakaş, Research on structural, spectral (IR, UV-Vis, 1H- and 13C-NMR) and light emitting properties of triisocyano-based trinuclear Au(I) complexes, Chem. Pap. 74 (2020) 2415–2425, https://doi.org/10.1007/s11696-020-01088-3.
[33] A. Irfan, S. Muhammad, A.R. Chaudhry, A.G. Al-Sehemi, R. Jin, Tuning of optoelectronic and charge transport properties in star shaped anthracenothiophene-pyrimidine derivatives as multifunctional materials, Optik (Stuttg). 149 (2017) 321–331, https://doi.org/10.1016/j.ijleo.2017.09.065.
[34] H.H. Khalid, S. Erkan, N. Bulut, Halogens effect on spectroscopy, anticancer and molecular docking studies for platinum complexes, Optik (Stuttg). 244 (2021), 166324, https://doi.org/10.1016/j.ijleo.2021.166324.
[35] S. Erkan, D. Karakaş, DFT investigation and molecular docking studies on dinuclear metal carbonyls containing pyridyl ligands with alkyne unit, Chem. Pap. 73 (2019) 2387–2398, https://doi.org/10.1007/s11696-019-00784-z.
[36] harald hillebrecht and wolfgang brütting by michael cölle, jürgen gmmeiner, wolfhang milius, Preparation and characterization of, Adv. Mater. 21 (2003) 1769–1773. https://doi.org/10.1002/adfm.200390015.
[37] H. Xin, M. Guang, F.Y. Li, Z.Q. Bian, C.H. Huang, K. Ibrahim, F.Q. Liu, Photoluminescence and electroluminescence of the exciplex formed between a terbium ternary complex and N, N′-diphenyl-N, N′-bis(3-methylphenyl)-1,1′-diphenyl-4,4 ′-diamine, Phys. Chem. Chem. Phys. 4 (2002) 5895–5898, https://doi.org/10.1039/b207990a.
[38] C.Y. Kwong, A.B. Djurišić, W.C.H. Choy, D. Li, M.H. Xie, W.K. Chan, K.W. Cheah, P. T. Lai, P.C. Chui, Efficiency and stability of different tris(8-hydroxyquinoline) aluminium (Alq3) derivatives in OLED applications, Mater. Sci. Eng. B Solid-State Mater. Adv. Technol. 116 (2005) 75–81, https://doi.org/10.1016/j.mseb.2004.09.024.
[39] S. Nath, S.K. Pathak, B. Pradhan, R.K. Gupta, K.A. Reddy, G. Krishnamoorthy, A. S. Achalkumar, A sensitive and selective sensor for picric acid detection with a fluorescence switching response, New J. Chem. 42 (2018) 5382–5394, https://doi.org/10.1039/C7NJ05136K.
[40] A. Mishra, R. Dheepika, P.A. Parvathy, P.M. Imran, N.S.P. Bhuvanesh, S. Nagarajan, Fluorescence quenching based detection of nitroaromatics using luminescent triphenylamine carboxylic acids, Sci. Rep. 11 (2021) 19324, https://doi.org/10.1038/s41598-021-97832-0.
[41] O. Gungor, M. Kose, Selective detections of nitroaromatic explosives by monomeric and polymeric Bi(III) complexes, Sensors Actuators, B Chem. 264 (2018) 363–371, https://doi.org/10.1016/j.snb.2018.02.184.